Solvent and Protein Effects on the Vibrational Frequency Shift and Energy Relaxation of the Azide Ligand in Carbonic Anhydrase

Mireia Garcia-Viloca,[†,‡] Kwangho Nam,[†] Cristóbal Alhambra,[†,§] and Jiali Gao*[,†]

Department of Chemistry, Supercomputing Institute, and Digital Technology Center, University of Minnesota, Minneapolis, Minnesota 55455, and Institut de Biotecnologia i Biomedicina, Universitat Autònoma de Barcelona, 08193 Bellaterra, Spain

Received: June 8, 2004

Combined QM/MM molecular dynamics simulations have been carried out to investigate the vibrational frequency shift for the azide antisymmetric stretch mode induced by aqueous solvation and by carbonic anhydrase II. In this work the oscillator and the enzyme active site is treated explicitly by quantum mechanics. Thus, the dynamical change of the potential energy surface of the oscillator can be adequately represented. We found that although the average geometry of the azide ion is symmetric in aqueous solution, the instantaneous solute−solvent interactions induce localization of the resonance structure having triple bond character, leading to a blue shift in the observed antisymmetric vibrational frequency in polar solvents. The computed frequency shift of azide ion from water to the active site of carbonic anhydrase is 56 cm^{-1}, in good accord with the experimental value of 51 cm^{-1}. Analyses of the computational results demonstrate that the origin of the protein-induced blue shift is due to a combination of ligand binding to the zinc ion and protein dynamical interactions. The former makes the dominant contribution by stabilizing the $N{\equiv}N^{+}-N^{2-}$ ionic state through ligand−metal coordination, whereas the latter attenuates the ligand−metal bonding interactions, recovering some of the $N^{-}{=}N^{+}{=}N^{-}$ valence bond character. Furthermore, the vibrational energy relaxation time has been determined both in water and in the enzyme. Intramolecular vibrational redistribution provides the main doorway for energy relaxation of the azide antisymmetric stretch in the enzyme, which is consistent with that obtained previously for an azide ion in water by Morita and Kato. Following this mechanism coupled with the quantum correction factor suggested by Skinner and Park, we obtained vibrational relaxation times of about 2 ps in water and 6 ps in carbonic anhydrase. Importantly, the change in relaxation time by a factor of 2.5 from water to the enzyme active site is in good accord with experiment.

1. Introduction

Protein dynamics encompasses a wide range of time and length scales that are essential to biological functions including ligand binding, energy transfer, and catalysis.[1,2] In principle, chemical reaction can be controlled by energy fluctuations of the substrate in the enzyme active site, especially when the chemical process involves charge translocations.[3] These fluctuations, which occur in the time scale of nuclear motions, can affect the electrostatic environment of the active site, which in turn can modulate the energies of the reactant and product states, leading to the stabilization of the transition state. A powerful experimental approach to determining properties of protein dynamics is the use of femtosecond spectroscopy.[3−6] Recently, Hochstrasser and co-workers used a three-pulse echo technique to determine the fluctuations in vibrational frequency of small molecules and ions in proteins.[7] These experiments provide a direct probe of the dynamic interactions between the ligand and its environment since molecular vibrations are sensitive to the change of the potential energy surface of the oscillator due to fluctuations of the electrostatic environment. Lim et al. found that the antisymmetric vibration of an azide ion in carbonic anhydrase II (CA-II) is blue-shifted by 50 cm^{-1} relative to that in water.[7] Furthermore, the vibrational relaxation time T_1 is also increased by a factor of more than 2 from water (1.2 ps) to the enzyme (2.8 ps). Complementing these experimental studies, we report molecular dynamics simulations of an azide ion in water and in CA-II using a combined quantum mechanical and molecular mechanical (QM/MM) potential that explicitly takes account of the dynamical changes in the potential energy function due to ligand−protein interactions.

The small triatomic ion N_3^- has been extensively used as a molecular probe to study vibrational dynamics in condensed phases.[7−20] The fast vibrational energy relaxation time (0.8 to 1.2 ps)[7,19] and frequency shift[9,21,22] of the antisymmetric stretch mode (ω_3) in water are strong indications of electrostatic interactions between the ion and solvent. The dynamics of azide ion has also been studied in micelle solutions, in which the relaxation time increases with increasing micelle concentration.[19,20,23] The fundamental vibrational frequencies have been investigated theoretically.[9,17,24−26] Classical molecular dynamics simulations of an azide ion in water were first carried out by Ferrario et al.,[27] who showed that the computed relaxation times for azide ion in water and in methanol are sensitive to the potential energy functions used, particularly on charge distribution of the ion. These authors obtained a rotational correlation time in good agreement with experiment, but the calculated vibrational relaxation time was greater (∼10 ps) than the experimental value.[27] Later, the antisymmetric vibrational

[†] University of Minnesota.
[‡] Universitat Autònoma de Barcelona.
[§] Present address: CNS-Chemistry, AstraZeneca Pharmaceuticals LP, Wilmington, DE 19850-5437.

10.1021/jp047526g CCC: $27.50
Published on Web 08/10/2004

frequency shift was calculated to be 80 cm^{-1} from gas phase to aqueous solution using ab initio molecular dynamics,[28] in accord with experiment. Recently, Morita and Kato have extended these calculations to study vibrational energy relaxation by including intramolecular vibrational redistribution (IVR) and charge polarization for the azide ion.[29] They found that IVR provides an important mechanism of vibrational relaxation of azide ion in aqueous solution.[29]

The wave function of the azide ion can be described by the admixture of three dominant valence bond (VB) structures:

$$\underset{\mathbf{1}}{N^{2-}-N^{+}\equiv N}, \quad \underset{\mathbf{2}}{N^{-}=N^{+}=N^{-}}, \quad \underset{\mathbf{3}}{N\equiv N^{+}-N^{2-}}$$

The primary contributor to the total wave function in the gas phase is the second configuration, **2**, which has formal charges of −1 au on both terminal nitrogen atoms, and +1 au on the central (N2) atom. In polar solvents, the "ionic" structures **1** and **3** can be stabilized by specific hydrogen-bonding interactions. Consequently, the instantaneous interactions with a given solvent configuration can lead to localization of any one of the VB structures, resulting in different potential energy surfaces and vibrational frequencies. The increased triple bond character in structures **1** or **3** in polar solvent gives rise to an observed blue shift in the antisymmetric vibrational frequency. When the azide ion is complexed to a Zn^{2+} ion in carbonic anhydrase, the VB structure **1** (or **3** depending on which terminal nitrogen binds the metal center) will be stabilized along with charge transfer to the metal center. The specific interactions of the Zn-bound azide ligand with the neighboring amino acid residues in the active site of CA-II will further influence the functional form, the potential energy surface, and, thus, the vibrational frequencies of azide in the enzyme. Lim et al. attributed the observed blue shift in azide ω_3 vibration in CA-II relative to that in water (50 cm^{-1}) to the increased admixture of the triple-bonded VB structure **1**.[7] On the basis of the X-ray structure,[12,13] they proposed that Thr199 plays an important role in modifying the potential energy surface and modulating the charge fluctuation of the Zn-bound azide.[7]

Carbonic anhydrase II (CA-II) is a metalloenzyme that catalyzes the interconversion of CO_2 and bicarbonate. The X-ray structure of the CA-II−azide complex shows that the active site lies in the bottom of a deep cavity in the protein (about 10 Å from the protein surface), which contains a Zn^{2+} ion, coordinated in an approximately tetrahedral geometry to four ligands: azide ion, His94, His96, and His119.[12,13,30] In the catalytic cycle, a water molecule is bound to the metal center in place of the azide ion. The water molecule is activated by proton transfer through a network of hydrogen bonds to generate a hydroxide ion for the nucleophilic attack of carbon dioxide.[31−40] The azide ion is a competitive inhibitor of the formation and dehydration of bicarbonate in CA-II.[12,13,41] Because of its biological importance as a CO_2 carrier, numerous computational studies of CA-II have been performed, especially on the initial proton transfer process[31−40] and the reaction mechanism.[42−50] Protein effects on charge distribution have been investigated by Merz and Banci who carried out molecular dynamics simulations of N_3^- in CA-II, employing a combined QM/MM potential.[41,51] The results from that calculation indicated, however, that configuration **2** is actually favored in the enzyme active site.[41]

Parallel to the exciting experiments of Lim et al.,[7] which revealed dynamic properties of the aqueous solvent and the active site of CA-II enzyme through their effects on molecular vibrations (mean values and time-correlation functions), we have performed molecular dynamics simulations using a combined QM/MM potential.[52−57] Our approach has the advantage of using a quantum mechanical force field directly for the description of the active site, including the oscillator. By virtue of an explicit QM treatment of the probe molecule, the electronic polarization by the surrounding protein and solvent dynamics and the change of the potential energy surface are naturally included.[51,55,56,58,59] Although the goal of this work is not on the detailed reaction mechanism and drug design, these calculations provide new insights into the understanding of the mechanism of the frequency shift and vibrational energy relaxation of azide ion in water and in the active site of carbonic anhydrase II.

In this paper, we first describe the theoretical background and the procedures for parametrization of the combined QM/MM model. This is followed in section 4 by a summary of the computational details. Results and discussion are given in section 5. The paper concludes with a summary of major findings of the present study.

2. Theory

2.1. Combined QM/MM Potential. We employ a combined quantum mechanical and molecular mechanical (QM/MM) potential to describe the solute−solvent and the ligand−enzyme system. The method of combined QM/MM potentials has been reviewed elsewhere.[52,56,57,60] Here, we briefly summarize the essential terms and definitions used in the present discussion. For a hybrid QM and MM system, the effective Hamiltonian is given by

$$\hat{H}_{\text{eff}} = \hat{H}^0_{\text{qm}} + \hat{H}_{\text{qm/mm}} + \hat{H}_{\text{mm}} \tag{1}$$

where $\hat{H}^0_{\text{qm}}$ is the Hamiltonian for the QM subsystem, $\hat{H}_{\text{mm}}$ is the molecular mechanical potential of the MM subsystem, and $\hat{H}_{\text{qm/mm}}$ describes the interactions between the quantal and the classical parts of the system. The interaction Hamiltonian can be further divided into an electrostatic term and a van der Waals component,[52,56] in which the former accounts for the interactions between the electrons and nuclei of the QM subsystem and the partial atomic charges of the MM sites, and the latter is modeled by a Lennard-Jones form

$$\hat{H}^{\text{vdW}}_{\text{qm/mm}} = \sum_{s=1}^{S}\sum_{m=1}^{M} 4\epsilon_{sm}\left[\left(\frac{\sigma_{sm}}{r_{sm}}\right)^{12} - \left(\frac{\sigma_{sm}}{r_{sm}}\right)^{6}\right] \tag{2}$$

where M and S are, respectively, the total number of QM atoms and MM interaction sites, and r_{sm} is the distance of the QM atom m from the MM site s. The combining rules for eq 2 are $\sigma_{sm} = (\sigma_s + \sigma_m)/2$ and $\epsilon_{sm} = (\epsilon_s\epsilon_m)^{1/2}$, where σ_i and ϵ_i are empirical parameters for atom i. Standard force field parameters are used for σ_s and ϵ_s (vide infra),[61] whereas van der Waals parameters for the QM subsystem (σ_m and ϵ_m) can be optimized to obtain the best QM−MM interactions in comparison with experimental values or high-level ab initio calculations.[62,63]

For the CA-II enzyme system, we have used the generalized hybrid orbital (GHO) method to treat the covalent bonds across the QM region and the MM region.[64] In particular, the C_α atoms of the three histidine residues (His94, His96, and His119) that form the inner coordination sphere of the metal ion were defined as the GHO boundary atoms and the QM/MM partition for the CA-II system is depicted in Figure 1. Along with the azide ion and Zn^{2+} ion, a total of 40 atoms are included in the QM region. Note that we have used a somewhat larger QM system by placing the boundary atom at the C_α position, rather than the

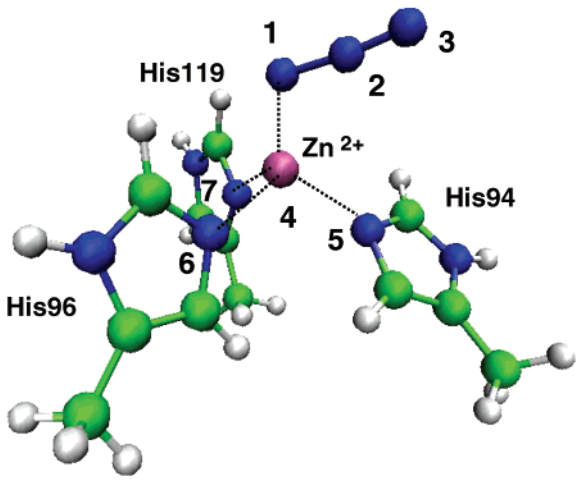

Figure 1. Optimized structure of the $[Zn(MeIm)_3-N_3]^+$ metal complex in the gas phase using the semiempirical PM3-AZI-ZN model. In the enzyme calculations, methylimidazoles are replaced by histidines and the GHO boundary atoms are located at the C_α positions.

typical choice of the C_β atom. Recent studies indicate that energetic results are more stable by using the larger QM region.[65]

2.2. Methods for Computing the Antisymmetric Frequency of the Azide Ion. We have used three different approaches to estimate the antisymmetric vibrational frequency of an azide ion in aqueous solution and in carbonic anhydrase. The first method makes use of the harmonic approximation for the potential energy surface, while the other two methods (one-dimensional Schrödinger equation and the Fourier transform of the time-correlation functions of the antisymmetric coordinate) take into account anharmonicity.

2.2.1. Normal Mode Analysis. Harmonic frequencies, ω_3, were determined for an azide ion in the gas phase, ligated to $[Zn(MeIm)_3]^{2+}$, in water, and in the active site of CA-II. For the first two cases, normal mode analyses (NMA) were performed using the corresponding energy minima optimized at several theoretical levels. The Gaussian 98[66] and Mopac 5.09m[67] packages, and the Charmmrate module[68] of Charmm (c29a2)[69] have been used for these calculations. For azide in water and in CA-II, we have used a frozen bath (or embedded cluster) approximation,[70] in which we optimized the geometry of the azide ion in the field of the remainder of the system (water or enzyme) kept fixed at the instantaneous configurations along the molecular dynamics trajectory. In geometry optimization of the azide ion, the center of mass coordinate and the rotations of azide are fixed at the instantaneous value as well. Then, for each of the located minima, we performed a normal mode calculation for the azide ion under the potential field of the rest of the system. Since rotations and translations of the azide ion in condensed phases are hindered, all modes have none-zero frequencies; the 6 lowest frequency modes correspond to libration motions.

2.2.2. One-Dimensional Vibrational Schrödinger Equation. The antisymmetric stretch vibrational frequency of azide ion was also determined by solving the one-dimensional Schrödinger equation, which is denoted as 1DW in the following discussion, along the normal coordinate

$$q_3 = \frac{1}{\sqrt{2}}(r_1 - r_2) \tag{3}$$

where r_1 and r_2 are the two N−N bond distances of azide. The Hamiltonian for the antisymmetric vibration is

$$\hat{H}_v(q_3) = -\frac{\hbar^2}{2\mu_3}\frac{d^2}{dq_3^2} + V(q_3) \tag{4}$$

where μ_3 is the reduced mass associated with q_3, and $V(q_3)$ is the potential energy as a function of q_3. In the present study, $V(q_3)$ is numerically determined for a set of 13 values of q_3 (one at the minimum q_3^o and six points on each side of the minimum separated at $\Delta q_3 = 0.04$ Å between two neighboring points) using the combined QM/MM potential at an instantaneous configuration in the dynamics simulation (see below), and then $V(q_3)$ is fitted to an analytical cubic spline function.[71]

The vibrational eigenvalues, E_n, and eigenfunctions, Ψ_n, are obtained by solving the one-dimensional nuclear Schrödinger equation

$$\hat{H}_v(q_3)\Psi_n = E_n\Psi_n \tag{5}$$

where the nuclear wave function is represented as a linear combination of a set of Gaussian basis functions.[72] The exponent parameter α in the Gaussian basis functions has been chosen following the criteria explained in ref 72. In this work, the basis functions have been distributed at equally spaced points $q_{3,i}$ within the interval of q_3 where $V(q_3)$ has been determined numerically. We have verified the convergence of the results obtained with different number of basis functions, and the final value used for α is 6000 Å^{-2} and the number of Gaussian basis functions is 75.

The reduced mass associated with the reaction coordinate q_3 for each of the optimized configurations of azide in a given environment is calculated as

$$\mu_3 = \frac{m_N}{2 - \cos\theta} \tag{6}$$

where m_N is the mass of nitrogen (14.007 au) and θ is the instantaneous N1−N2−N3 bond angle, which is very close to 180°. This corresponds to the assumption that the azide ion has at least a C_{2v} symmetry, but at any instantaneous solvent configuration, this is certainly not generally satisfied. Nevertheless, in view of the relatively small fluctuations in the azide geometry, we have adopted this simple expression to evaluate the reduced mass associated with the antisymmetric stretch coordinate.

We have used the Gaussian 98 program[66] to calculate the one-dimensional potential energy profiles $V(q_3)$ for an azide ion in the gas phase and in the $[Zn(MeIm)_3-N_3]^+$ complex at the ab initio and DFT levels of theory. In addition, we have used a modified version of CHARMM (c29a2)[69] to calculate the $V(q_3)$ profiles for these two gas phase species using the semiempirical model and for azide in water and in the active site of CA-II using a combined QM/MM Hamiltonian.

2.2.3. Time-Correlation Functions. The time-correlation function of the fluctuation of the antisymmetric coordinate of azide, which contains information of the change in potential energy surface due to dynamic fluctuations of the solvent and the protein, can be Fourier transformed into the frequency-domain to yield the vibrational frequency[73,74] of the antisymmetric stretch mode of azide ion in water and in CA-II. The normalized autocorrelation function (ACF) of the fluctuations of $q_3(t)$, $\delta q_3(t) = q_3(t) - \langle q_3\rangle$, is calculated as follows

$$C_{33}(\tau) = \frac{\langle \delta q_3(\tau)\delta q_3(0)\rangle}{\langle \delta q_3(0)\delta q_3(0)\rangle} \tag{7}$$

Since eq 7 is a classical TCF, only the real part of the Fourier transform is evaluated.

$$\hat{I}(\omega) = 2\int_0^\infty \mathrm{d}t\, C_{33}(t)\cos\omega t \tag{8}$$

2.3. Vibrational Energy Relaxation. The time evolution of the excess vibrational energy dissipation can be described by the exponential decay law[75]

$$\frac{\langle E_v(t)\rangle - \langle E_v(\infty)\rangle}{\langle E_v(0)\rangle - \langle E_v(\infty)\rangle} = \mathrm{e}^{-t/T_1} \tag{9}$$

where T_1 is the vibrational relaxation time, $\langle E_v(t)\rangle$ is the nonequilibrium average of the vibrational energy at time t, and $\langle E_v(\infty)\rangle$ is generally assumed to have the thermal value k_BT. In principle, T_1 can be determined through molecular dynamics simulations, beginning with a specified value of $\langle E_v(0)\rangle$, as shown by Whitnell et al. in their study of the vibrational relaxation of methyl chloride in water.[76,77] In the present study, we estimate the relaxation time by computing the classical force autocorrelation function on a selected vibrational mode in the protein and aqueous environment. This approach has been used in a variety of studies of vibrational energy relaxation in condensed phases,[78−87] and we follow closely a procedure described by Straub and co-workers for the study of vibrational relaxation in protein environments.[85−88]

In this treatment, the total Hamiltonian of the system is partitioned into three terms: $H = H_v + H_b + V_{vb}$, where H_v is the vibrational Hamiltonian for the excited mode of the oscillator with eigenstates and energies of $|n>$ and E_n ($n = 0, 1, ...$), H_b is the bath Hamiltonian for the rest of the system, and V_{vb} describes the interaction between the oscillator and the bath. If q is the coordinate for the vibrational mode of interest, V_{vb} is often expanded in powers of q, and only the linear term is kept so that $V_{vb} \approx -qF_q$, where F_q, which is, of course, a function of the bath coordinates, is the force exerted on q. Then, the Fermi golden rule rate constant for transition from the $n = 1$ state to the $n = 0$ state is[78,83]

$$k_{1\to 0} = \frac{|q_{10}|^2}{\hbar^2}\int_{-\infty}^{\infty} \mathrm{d}t\, \mathrm{e}^{\mathrm{i}\omega t}\langle F_q(t)F_q(0)\rangle_{qm} \tag{10}$$

where $q_{10} = \langle 1|q|0\rangle$, $\omega = (E_1 - E_0)/\hbar$, and $\langle F_q(t)F_q(0)\rangle_{qm}$ is the fully quantum mechanical force−force time-correlation function (TCF). For a harmonic oscillator, $|q_{10}|^2 = \hbar/2\mu\omega$. Assuming that the quantum mechanical TCF can be replaced by its classical analogue, the rate constant is then approximated by[84]

$$k_{1\to 0} \approx Q(\omega)\frac{|q_{10}|^2}{\hbar^2}\int_{-\infty}^{\infty} \mathrm{d}t\, \mathrm{e}^{\mathrm{i}\omega t}\langle \delta F_q(t)\delta F_q(0)\rangle_{cl} \tag{11}$$

where a quantum correction factor (QCF), $Q(\omega)$, is introduced,[84] and the classical force−force TCF, $\langle \delta F_q(t)\delta F_q(0)\rangle_{cl}$, can be determined through molecular dynamics simulations. The scalar force on the vibration coordinate q is obtained by a projector method

$$F_q = -\frac{\partial V}{\partial q} = -\left(\frac{\partial V}{\partial \mathbf{R}}\right)\cdot\left(\frac{\partial \mathbf{R}}{\partial q}\right) \tag{12}$$

where $\mathbf{R}$ represent the Cartesian coordinates of all atoms in the system.

Skinner and Park suggested that $Q(\omega)$ should be determined on the basis of the mechanism of the vibrational relaxation.[84,86] In the case that the vibrational energy of a vibrational mode of frequency ω is transferred to a dominant bath mode of frequency ω_i and the remainder, $\omega - \omega_i$, to a low-frequency harmonic vibration or translations and/or rotations of the bath molecules, the quantum correction factor is[84]

$$Q(\omega) = Q_H(\omega_i)Q_{HS}(\omega - \omega_i) \tag{13}$$

where the harmonic QCF is given by[78,79]

$$Q_H(\omega_i) = \frac{\hbar\omega_i/k_BT}{1 - \mathrm{e}^{-\hbar\omega_i/k_BT}} \tag{14}$$

and the harmonic/Schofield QCF is given by[84,89]

$$Q_{HS}(\omega) = \mathrm{e}^{\hbar\omega/4k_BT}\sqrt{\frac{(\hbar\omega/k_BT)}{1 - \mathrm{e}^{-\hbar\omega/k_BT}}} \tag{15}$$

A special case is for energy transfer to a resonant bath mode, in which $\omega = \omega_i$, and thus, $Q(\omega) = Q_H(\omega)$ since $Q_{HS}(0) = 1$.

By treating the Hamiltonian H_v as a harmonic oscillator for the vibrational mode, and using $Q(\omega) = Q_H(\omega)$, the relaxation time can be expressed by the Landau−Teller formula

$$\frac{1}{T_1} = k_{1\to 0} = \frac{1}{\mu k_BT}\int_0^\infty \mathrm{d}t\cos(\omega t)\,\langle \delta F_q(t)\delta F_q(0)\rangle_{cl} \tag{16}$$

where μ is the reduced mass of the oscillator. Equation 16 is the uncorrected classical estimate of the vibrational relaxation rate based on the first-order time-dependent perturbation theory.[75,78] Bader and Berne showed that the remarkable feature of eq 16 is that the relaxation time for a classical solute in a classical solvent, which can be determined through classical molecular dynamics simulations, is identical to that for the quantum oscillator in the quantum bath for the harmonic model.[79]

3. Parametrization of the Potential Energy Function

We use a combined quantum mechanical and molecular mechanical (QM/MM) potential to treat the ligand−protein−solvent system.[55] Although it is possible to carry out combined QM/MM simulations by treating a small solute like azide ion with ab initio molecular orbital or density function theory (DFT) in the aqueous system,[74,90−92] they are not feasible for the enzyme dynamics calculations, even with a modest basis set (such as the split valence 3-21G basis). In the enzyme CA-II, a total of 40 QM atoms (Figure 1) must be included. We have adopted the semiempirical parametrized model 3 (PM3)[93] method for the description of the QM region. The MM part of the system is approximated by the CHARMM22 force field[61] for the enzyme and the TIP3P model for water.[94] However, the accuracy of semiempirical methods often needs to be improved in order to obtain quantitative results as is the case for computing the vibrational frequencies of azide ion using PM3. To this end, we have developed a set of specific parameters (called SRP) for the molecular vibration of azide ion.

It should be emphasized that the optimization of the semiempirical QM model is based on comparison of gas phase properties for the azide ion and the zinc cluster with experimental and high-level ab initio results. The aim of this parametrization process is to improve the intrinsic performance of the QM model for the description of an isolated azide ion or in the metal complex in the *gas phase*. The effects of solvation

TABLE 1: Modified Semiempirical PM3 Parameters for Azide Ion (PM3-AZI) and for Azide−Zn^{2+} Interactions (PM3-AZI-ZN)[a]

parameters	PM3	PM3-AZI/PM3-AZI-ZN
β_p (eV)	−20.04	−22.50
F_{31} (Å)	1.711	1.750
$\beta_{p(N)p(Zn)}$ (eV)	−13.20	−17.0
$\beta_{p(N)s(Zn)}$ (eV)	−10.38	−28.0
$\beta_{s(N)p(Zn)}$ (eV)	−10.21	−3.00
$\beta_{s(N)s(Zn)}$ (eV)	−7.39	−1.00
$U_{pp(Zn)}$ (eV)	−11.05	−10.0

[a] The remaining semiempirical parameters are kept the same as the original PM3 model.

TABLE 2: Computed and Experimental Antisymmetric Vibrational Frequencies ω_3 for Azide Ion and for the Zinc Complex $[Zn(MeIm)_3-N_3]^+$ in the Gas Phase[a]

	NMA			1DW		
method	azide	complex	$\Delta\omega_3$	azide	complex[b]	$\Delta\omega_3$
PM3	2486	2417	−69	2449		
HF/6-31+G(d)	2206	2405	199	2138		
B3LYP/6-31+G(d)	2088	2203	115	2029	2162	133
PM3-AZI-ZN	2037	2209	172	2048	2215	167
exptl	1987			1987		

[a] The optimized semiempirical model PM3-AZI-ZN is used, while the vibrational frequencies are determined by normal mode analysis (NMA) and by solving the one-dimensional vibration Schrödinger equation (1DW). Frequencies are given in cm^{-1}. The computed normal mode and 1DW antisymmetric frequencies for azide ion are 2147 and 2121 cm^{-1} at the MP2/6-31+G(d) level. [b] The 1DW calculations at the Hartree−Fock and PM3 levels did not seem to converge for the zinc complex structure, and we have not further analyzed this problem. For the comparisons discussed in the text, the normal mode frequencies are sufficient.

and protein dynamics on vibrational properties (shifts and relaxation rate) are not part of the parametrization.

3.1. The Azide Ion. Test calculations for an azide ion in gas phase show that neither AM1[95] nor PM3[93] methods were able to reproduce the experimental geometry and vibrational frequencies.[9] Both AM1 and PM3 methods underestimate the N−N distance by 0.02 Å and overestimate the antisymmetric vibrational frequency ω_3 by 637 and 500 cm^{-1}, respectively. Thus, to improve the potential energy surface without increasing the computational cost of the calculations, we adjusted some of the PM3 parameters for the nitrogen atom in azide ion against the experimental and high-level ab initio and DFT values for ω_3 and the N−N bond distance. We found that it was possible to improve the calculated antisymmetric vibrational frequency ω_3 without altering the charge distribution in the molecule simply by modifying just one parameter of a Gaussian function in the core−core term. To balance the results on the N−N bond lengths, we also adjusted the resonance integral parameter, β_p. The final parameters are listed in Table 1 (PM3-AZI model).

The performance of the optimized PM3 Hamiltonian for azide ion, which involves adjusting only two semiempirical parameters, is significantly improved over the original PM3 model in comparison with the experimental results (Table 2). The computed harmonic frequency is 2037 cm^{-1} for the antisymmetric stretch, while inclusion of anharmonicity by solving the one-dimensional Schrödinger equation along the ω_3 normal coordinate increases it to 2048 cm^{-1}. Overall, the computed antisymmetric stretch frequency using the modified PM3 model is similar to that computed at the B3LYP/6-31+G(d) level, which are 2088 and 2029 cm^{-1} from NMA and 1DW, respectively. The SRP-PM3 result deviates from the experimental value (1987 cm^{-1}) by only 3%.[9] For another comparison, the harmonic frequency (2147 cm^{-1}) and the 1DW value (2121 cm^{-1}) are too large from MP2/6-31+G(d) calculations in comparison with experiment. The optimized N−N bond distance from the modified PM3 model is somewhat too long by 0.06 Å compared to experiment (Table 3); however, it appears to be reasonable compromise at this point to achieve the aim of the present study.

TABLE 3: Computed and Experimental Bond Lengths for Azide Ion and for the Zinc Complex $[Zn(MeIm)_3-N_3]^+$ in the Gas Phase[a] (see Figure 4 for atomic numbers)

	N_3^-	$[Zn(MeIm)_3-N_3]^+$					
	r_{NN}	r_{12}	r_{23}	r_{14}	r_{45}	r_{46}	r_{47}
PM3	1.169	1.224	1.139	1.983	2.035	2.029	2.040
HF/6-31+G(d)	1.156	1.198	1.114	1.974	2.078	2.080	2.082
B3LYP/6-31+G(d)	1.190	1.215	1.155	1.972	2.047	2.050	2.053
PM3-AZI-ZN	1.246	1.358	1.173	1.802	2.155	2.139	2.148
exptl[b]	1.1884						

[a] All distances are given in angstroms. The N−N bond length for azide is 1.220 Å from MP2/6-31+G(d) optimizations. [b] Reference 9.

3.2. The $[Zn(MeIm)_3-N_3]^+$ Complex. In parallel, we computed the antisymmetric stretch frequency of azide in the metal complex $[Zn(MeIm)_3-N_3]^+$ (Figure 1), which is the simplest gas phase model for the active site of CA-II. Examination of this model is useful to assess the intrinsic properties of azide−metal interactions, which can be used as a reference to understand the effects of protein dynamics. To this end, we have adjusted the core integral parameter U_{pp} for zinc ion, and the one-electron resonance (β_s and β_p) integrals[93,95] between the nitrogen atoms in azide and Zn to improve the semiempirical description of the metal−ligand coordination interactions.[96] In standard semiempirical calculations, the one-electron resonance integral between basis orbitals μ and λ on atoms A and B, respectively, is assumed to be proportional to the overlap integral of the two atomic orbitals by $\beta_{\mu\lambda} = {}^1/_2(\beta_\mu + \beta_\lambda)S_{\mu\lambda}$.[93,95] In the present study, we decided to treat the four individual atomic orbital pairs ($\beta_{p(N)p(Zn)}$, $\beta_{p(N)s(Zn)}$, $\beta_{s(N)p(Zn)}$, and $\beta_{s(N)s(Zn)}$) independently. This approach has been used previously by Corchado et al. in their study of the kinetics of hydrocarbon free radical reactions[97] and in the parametrization of the self-consistent-charge tight-binding density functional (SCC-DFTB) method.[98] To control the amount of charge transfer between azide ion and Zn^{2+} by comparison with Mulliken population charges from HF/6-31+G(d) and B3LYP/6-31+G(d) calculations, the U_{pp} parameter for Zn^{2+} has been decreased slightly (less than 10% of the original PM3 value). The final model used for the $[Zn(MeIm)_3-N_3]^+$ complex is denoted as PM3-AZI-ZN, which includes the optimized PM3 for azide and the new resonance integrals for describing azide−Zn interactions. These parameters are included in Table 1. Note that the nitrogen atoms in the imidazole moiety are treated by the original PM3 model.

Table 2 shows the computed frequencies and shifts relative to the gas phase value obtained using various methods. The computed ω_3 values using the NMA and 1DW method at the B3LYP/6-31+G(d) level and the harmonic frequency from HF/6-31+G(d) are blue-shifted by about 120 to 200 cm^{-1}, which is greater than the frequency shift (110 cm^{-1}) on transferring azide ion from the gas phase into in the enzyme.[7] The original semiempirical PM3 Hamiltonian yields a computed shift of −69 cm^{-1} for the complex, in contrast to ab initio and DFT results. The present PM3-AZI-ZN model reproduces the blue shift predicted by ab initio and DFT calculations, with an estimated value of 167 cm^{-1}. The optimized geometrical parameters for the azide−metal complex are given in Table 3. In comparison

with ab initio and DFT results, the PM3-AZI-ZN model yields reasonable bond lengths in the $[Zn(MeIm)_3-N_3]^+$ complex.

3.3. QM/MM Interactions. Nonbonded interactions between the QM and MM regions consist of both electrostatic and van der Waals terms (eq 2). While the former is included in the electronic structure calculation, the latter term is represented empirically by the Lennard-Jones potential. Naturally, the force field parameters for MM atoms are kept unchanged, but the Lennard-Jones parameters for the QM atoms can be adjusted to yield the best description of QM/MM interactions. Previously, we have optimized the nonelectrostatic terms in QM/MM potentials by examining hydrogen-bonding interactions of bimolecular complexes and free energies of solvation of small compounds and recommended a set of parameters for semiempirical AM1[55,62] and HF/3-21G QM/MM calculations.[63] We have used the Lennard-Jones parameters optimized for semiempirical QM/MM simulations in the present study.[55] In addition, the azide van der Waals parameters have been optimized ($\sigma_N = 1.850$ Å, $\epsilon_N = 0.200$ kcal/mol) by comparison with B3LYP/6-31+G(d) results on interaction energy and geometries for the azide−water complex. Overall, the QM/MM interaction energies are within 1 kcal/mol of the corresponding ab initio data for bimolecular interactions.[55,62]

4. Computational Details

4.1. Azide Ion in Water. Molecular dynamics simulations have been carried out for an azide ion in water to determine solvent effects on the antisymmetric vibrational frequency shift and vibrational energy relaxation. Periodic boundary conditions (PBC) were used for a system consisting of one azide ion and 1728 water molecules in a box of about $37 \times 37 \times 37$ Å^3. Initially, the isothermal−isobaric (NPT) ensemble at 298 K and 1 atm was used to equilibrate the system with the MM force field to obtain an average equilibrium volume dimension. We used the leapfrog integration scheme[99] to propagate the equations of motion at a time step of 1 fs during the heating and equilibration stage along with the extended system constant pressure and temperature algorithm implemented in charmm.[100−102] All bond lengths and angles involving hydrogen atoms were constrained by the SHAKE algorithm,[103] and the dielectric constant was set to 1. The temperature of the system was gradually raised from 0 to 298 K in 30 ps of molecular dynamics, with the azide molecule under harmonic restraints. Then, the harmonic restraints on the azide were gradually released during a further 100 ps simulation at 298 K. The average length of the box edge in the last 5000 steps (5 ps) of the 100 ps run was 36.77714 Å, which was used in subsequent QM/MM molecular dynamics simulations at constant volume and temperature.

The QM/MM simulations for the azide ion in aqueous solution were performed using periodic boundary conditions at constant temperature and volume. The velocity Verlet integrator[104] and the Nosé−Hoover[100,101] constant temperature algorithm were used in these calculations at 298 K on the QM(PM3-AZI)/MM potential energy surface. After 20 ps of restrained MD simulations, with a harmonic term applied on the azide molecule using a force constant of 1 kcal mol^{-1} Å^{-2}, the system was allowed to move freely for 10 ps. Then, the time step was decreased to 0.2 fs and 100 ps molecular dynamics simulations were carried out. The structural data needed to calculate the vibrational frequency shift of azide in aqueous solution was taken from the last 5 ps (25 000 steps) of the simulation, during which the coordinates of the system were saved at every 100 steps and the azide coordinates were written out at every step. In all calculations using both MM and combined QM/MM potentials, a spherical cutoff distance of 13 Å was used for the nonbonded interactions along with a switch function between 12 and 13 Å to feather the interaction energy to zero. The nonbonded pair list and the image list were built on the basis of group separations, and they were updated every 25 steps and 100 steps, respectively.

4.2. Azide in the Active Site of Carbonic Anhydrase II. To model the coordination sphere of the active site in CA-II, the simplest gas phase model to study the properties of the active site is the tetracoordinated zinc complex, which was taken from the crystal structure of the ternary complex X-ray structure of the human carbonic anhydrase II system, containing Zn^{2+} and an azide ligand (PDB code: 1RAY).[12] The optimized structure for the $[Zn(MeIm)_3-N_3]^+$ complex, where MeIm is methylimidazole, is shown in Figure 1.

We used the same X-ray structure to build the azide-bound model for CA-II enzyme.[12] The crystal structure, 1RAY, contains 125 amino acid residues, 217 crystallographic water molecules, the Zn^{2+} ion, and an azide ion as the fourth ligand to the metal ion. The coordinates for all hydrogen atoms were generated using the HBUILD facility in CHARMM, and the protonation states for ionizable residues were set corresponding to neutral pH. Thus, histidine residues were modeled as neutral or protonated residues on the basis of possible hydrogen-bonding interactions in the X-ray crystallographic structure. Given the uncertainty of the protonation state of His64, which is located 9 Å away from the active site and has been proposed as the acceptor of a proton from the nucleophilic water bound to Zn^{2+} in CO_2 hydration,[105,106] we prepared two models of the Zn^{2+}−CA-II−azide system, one with His64 protonated and the other with a neutral His64. At this stage, the total charge inside of a sphere of 18 Å about the geometric center of the azide ligand was +7 e and +8 e for the neutral His64 model and the protonated His64 model, respectively. The excess charge in this sphere was neutralized by placing chloride anions near positively charged residues at distances greater than 12 Å from the active center. The resulting systems were further solvated with an 18 Å sphere of preequilibrated water molecules. Water molecules that are within 2.5 Å of any non-hydrogen atoms of the protein, ligand, cofactor, or chloride anions, and those that are outside of the 18 Å radius were removed. This procedure was repeated five times by randomly rotating the water spheres to solvate potential cavities of a single water configuration. Then, after a short molecular dynamics simulation of 5 ps to relax unfavorable contacts, the solvation process was repeated to fill in additional cavities generated during the equilibration dynamics.

Stochastic boundary molecular dynamics simulations (SBMD)[107,108] were performed to sample the configuration space of azide in the active site of CA-II. In this technique, the aqueous environment is mimicked by a sphere of water molecules centered and equilibrated around the active site. The rest of the system or reservoir zone is held fixed during the simulations, which provides a static field that supplies important electrostatic interactions of protein atoms in the reaction zone.[108] In the present study, the reaction zone contains the active site residues and all protein and solvent atoms within a sphere of 18 Å centered at the geometric center of azide. The reaction zone is further divided into the molecular dynamics region (containing the substrate, the metal, the enzymatic residues, water molecules, and anions within 14 Å of the center of the sphere), which is treated with Newtonian molecular dynamics, and the buffer region (from 14 to 18 Å), which represents a simplified heat bath and is treated by Langevin dynamics. Protein atoms are

TABLE 4: Calculated Antisymmetric Vibrational Frequency and Frequency Shift of Azide Ion in Water

	ω_3 (cm^{-1})		
method	gas	aqueous	$\Delta\omega_3$ (cm^{-1})
NMA	2037	2051.6 ± 0.3	15
1DW	2048	2073.8 ± 0.8	26
ACF	(2048)[a]	2086	38
exptl[a]	1987	2049	62

[a] 1DW value.

assigned to one or another region according to a reference structure at the beginning of the simulation and retained their labels throughout the simulation, whereas water molecules were allowed to diffuse between regions. A deformable boundary potential[107] was imposed on water molecules at the buffer/reservoir interface to represent the effect of bulk solvent outside this boundary. Additional details can be found in refs 108 and 59.

We note that the size of the reaction zone in the model described above is reasonable because the ligand of interest consist of only three atoms in the active site of CA-II enzyme. We tested different boundaries between the reaction and the reservoir zones, and the final model has a reasonable size of the reaction zone. Despite the simplicity of the model we obtained a good agreement with the experimental results, reassuring the use of the SBMD approach.

We used an integration time step of 1 fs during the heating and equilibration simulations. All bond lengths involving hydrogen atoms were constrained by the SHAKE algorithm.[103] Initially, we carried out 30 ps of QM(PM3-AZI-ZN)/MM SBMD simulations to heat the system to 298 K and then 50 ps more to equilibrate it at this temperature. From the final structure we ran further simulations with a smaller time step of 0.25 fs for 15 ps, followed by 18 ps of SBMD with time step 0.15 fs. During the last 9 ps (60 000 steps) of the later simulation, the protein coordinates are saved at every 200 integration steps, and the azide coordinates are stored at every time step. The trajectory coordinates are used for structural and vibrational analysis. For comparison, we carried out SBMD simulations using the standard PM3 parameters[93] to represent the QM part of the two Zn^{2+}−CA-II−azide model systems (with His64 unprotonated and protonated, respectively). These simulations were run with exactly the same conditions as the protonated His64 model, except that the time step was 1 fs. Structural data for analysis were saved after the heating and equilibration stages at every 100 steps during 60 ps.

5. Results and Discussion

5.1. Solvent Effect on the Azide Antisymmetric Stretch Vibration. In the gas phase, azide ion has $D_{\infty h}$ symmetry and its electronic structure can be represented by the mixture of the three resonance structures, with equal structural weight on **1** and **3** (vide supra). In aqueous solution, the instantaneous interactions with the solvent perturb the mixing of these resonance structures. The observed increase in the ω_3 frequency of azide ion in H_2O and D_2O by 62 cm^{-1} and 56 cm^{-1}, respectively,[10,21] indicates that hydrogen-bonding interactions with the solvent stabilize the triple-bonded structures (**1** or **3**). The computed antisymmetric vibrational frequencies for azide in water from molecular dynamics simulations using periodic boundary conditions at 298 K and the combined QM(PM3-AZI)/MM potential along with that in the gas phase are listed in Table 4.

The average antisymmetric vibrational frequency $\langle\omega_3\rangle$ from normal mode analysis is 2052 cm^{-1} from structures saved during 10 ps molecular dynamics simulations. In comparison with the gas phase value of 2037 cm^{-1} using the PM3-AZI model, we obtain a harmonic frequency shift $\Delta\omega_3$ of 15 cm^{-1}, which is too small compared to experiment. In these calculations, we optimized the azide structure for each configuration by fixing the center of mass and rotation coordinates of the azide ion in the bath of the instantaneous solvent configuration, which is also frozen. We have calculated the one-dimensional QM/MM potential, $V(q_3)$, as a function of the antisymmetric normal mode coordinate for azide, q_3, for each of the 250 configurations saved during the last 5 ps of the PBC MD simulation. The numerical values for $V(q_3)$ were obtained in a similar way as the structure optimizations described above, except that the instantaneous angle of the azide ion is fixed as well at a given value of q_3. Thus, only one of the bond distances is an independent variable. The average value $\langle\omega_3\rangle$ from the 1DW calculations is 2074 cm^{-1}, which gives in an estimated frequency shift of 26 cm^{-1}. The 1DW method has the advantage of introducing anharmonicity of the potential energy surface, although the gas phase normal coordinate for azide ion was used to represent the antisymmetric stretch mode in water. This approximation neglects the contributions from cross terms in the potential and kinetic energy matrices, which lead to coupling with other vibration modes.

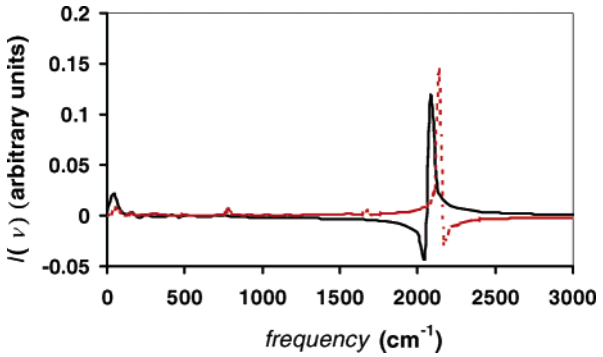

Figure 2. Power spectra of the time-correlation function of the antisymmetric stretch coordinate shown in Figure 3 for azide ion in water (solid line, black) and in carbonic anhydrase (dashed line, red).

The best estimate of the aqueous solvent effect on the antisymmetric vibrational frequency is obtained from the power spectrum of the autocorrelation function (ACF) of the fluctuating coordinate, averaged over the same trajectory that was used to calculate the average frequencies using the NMA and 1DW method (Table 4). In the ACF calculation, we have used all azide coordinates saved at every integration step. The Fourier transform of the ACF of the fluctuation in q_3 is given in Figure 2 (solid line). The calculated antisymmetric frequency is 2086 cm^{-1}, yielding an estimated blue shift of 38 cm^{-1} (using the 1DW gas phase value). The accord with experiment is reasonable as the ACF approach captures both anharmonicity of the potential surface and the coupling between internal vibrations and interactions with the solvent. Furthermore, the computed antisymmetric frequency from its Fourier transform is not very sensitive to the exact form of the fluctuating coordinate used.

Table 5 compares the gas phase Mulliken partial charges and the average values obtained over 100 ps of molecular dynamics simulations of azide in water along with the data for azide in the enzyme (see below). Under conditions of the present simulations, the electronic structure remains in the ground state. The calculated charges in water indicate that there is instantaneous asymmetry that localizes the valence bond structures **1**

TABLE 5: Average Mulliken Population Charges (au) for Azide Ion (N1−N2−N3)$^-$ in the Gas Phase, in Aqueous Solution, in the [Zn(MeIm)$_3$−N$_3$]$^+$ Complex, and in Carbonic Anhydrase

atom	gas phase	water[a]	[Zn(MeIm)$_3$−N$_3$]$^+$	CA-II[b]
N1	−0.880	−0.950 ± 0.083	−0.527	−0.534 ± 0.034
N2	0.761	0.885 ± 0.028	0.746	0.804 ± 0.025
N3	−0.880	−0.935 ± 0.084	−0.281	−0.393 ± 0.037

[a] Averaged over 500 000 steps of MD simulation with a time step of 0.2 fs. [b] Averaged over 60 000 steps of MD simulation with a time step of 0.15 fs.

or **3** since the average charges are not identical on the two terminal nitrogen atoms. Similarly, the average value of q_3 is essentially zero (0.00015 Å), indicating that the two N−N bond lengths are reasonably converged (1.2426 ± 0.0144 and 1.2424 ± 0.0138 Å), but the short-time asymmetry is reflected by the variance of the antisymmetric coordinate, which is 0.0231 Å. Thus, the asymmetry in geometry introduced by instantaneous solvation is noticeable, although small. This is consistent with the quasi-symmetric energy profile and vibrational wave functions obtained for these configurations.

5.2. Protein Effects on the Azide Antisymmetric Stretch Vibration. We first examine the effect of metal binding on the azide vibrational frequency. A noticeable change in the [Zn(MeIm)$_3$−(N$_3$)]$^+$ complex is the induction of asymmetry in the N−N bond distance of azide ion up on binding to the zinc atom (Table 3). Both HF and DFT calculations using the 6-31+G(d) basis set show that the distance between the nitrogen (N1) that is directly bound to Zn^{2+} and the central N2 nitrogen of azide ion (r_{12}) is elongated by 0.03 Å relative to the gas phase geometry. Concomitantly, the N2−N3 distance (r_{23}) is reduced by 0.04 Å (Table 3). This trend is reproduced using the present PM3-AZI-ZN model, though the predicted changes are somewhat greater than the ab initio data. The asymmetry in bond distances is a consequence of charge transfer from azide ion into the metal center and the migration of the azide electron density toward the N1 atom, leading to localization (or greater contribution) of resonance structure **1**. This is reflected by the partial Mulliken charges of azide in the metal complex (Table 5).

In the complex structure, the antisymmetric stretch vibration becomes predominantly the stretching mode of the N2−N3 bond, resulting in an increase in the ω_3 fundamental frequency. Table 2 shows that the harmonic frequency ω_3 for the azide moiety is blue-shifted in the metal complex by 115, 199, and 172 cm^{-1} from DFT, HF, and PM3-AZI-ZN calculations, respectively. Inclusion of anharmonicity by explicitly solving the one-dimension vibrational Schrödinger equation using the potential surfaces of B3LYP/6-31+G(d) and PM3-AZI-ZN models yields average blue shifts of 133 and 167 cm^{-1}, respectively. In this case, anharmonicity seems to have relatively small effects on the computed frequency shift for the cluster model. Experimentally, the azide antisymmetric vibrational frequency has been found to increase up on binding to alkali and alkaline metals in solution and it can have blue shifts as larger as 150 cm^{-1} in Mg(N$_3$)$_2$ crystal.[109]

Figure 3 depicts the calculated potential energy profile, the probability densities, and the energy levels of the first two vibrational states for N$_3^-$ (solid line) and [Zn(MeIm)$_3$−(N$_3$)]$^+$ (dotted line), respectively. The geometrical change of azide ion is reflected by a shift in the coordinate q_3 to a negative value. Figure 3 indicates that the increased steepness in the potential at negative values of q_3 leads to a greater splitting of the vibrational energy levels in the [Zn(MeIm)$_3$−(N$_3$)]$^+$ complex compared to azide ion in gas phase or in water.

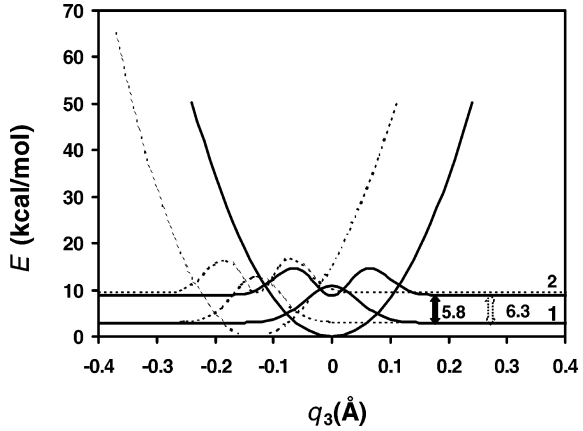

Figure 3. Potential energy profile, vibrational energy levels, and probability densities as a function of the antisymmetric stretch vibration coordinate, q_3, for azide in the [Zn(MeIm)$_3$−N$_3$]$^+$ metal complex (dotted line) and in carbonic anhydrase II at an instantaneous protein configuration during molecular dynamics simulations. The horizontal asymptotes of each $|\Psi_i|^2$curve lie just on the energy level (see the *y*-axis) corresponding to the vibrational state *i*.

TABLE 6: Average Bond Lengths (angstrom) and Bond Angles A_{xyz} (deg) at the Azide Binding Site in Carbonic Anhydrase[a]

	r_{12}	r_{23}	r_{14}	r_{45}	r_{46}	r_{47}	A_{214}	A_{145}	A_{416}	A_{417}
PM3[b]	1.20	1.15	2.02	2.02	2.06	2.12	130	112	120	113
PM3-AZI-ZN[c]	1.35	1.18	1.83	2.18	2.21	2.24	107	115	125	123
X-ray 1[d]	1.27	1.33	2.02	2.18	2.20	2.12	113	116	103	120
X-ray 2[e]			2.0	2.0	1.9	2.0		90	134	105

[a] Atom numbers are shown in Figure 4. [b] Averaged over 141 configurations during 14 ps of QM(PM3)/MM simulations with a time step of 1 fs. The standard errors are about 0.01−0.05 Å for distances and 3−7° for angles. [c] Averaged over 300 configurations during 9 ps of QM(PM3-AZI-ZN)/MM simulations with a time step of 0.15 fs. The standard errors are about 0.01−0.07 Å for distances and 3−6° for angles. [d] Reference 12. [e] Reference 30.

Calculations performed with a protonated His64 or a neutral His64 in the enzyme show that the frequency shift $\Delta\omega_3$ was not sensitive to the protonation state of this residue. Therefore, we only discuss the results obtained for the system that contains a protonated His64 residue.

The effects of protein dynamics and interactions with the azide ion in the active site attenuate the asymmetry induced by the local interactions with the [Zn(MeIm)$_3$]$^{2+}$ fragment. Key geometrical parameters of the active site averaged from combined QM(PM3-AZI-ZN)/MM molecular dynamics simulations along with experimental values from the X-ray structure are given in Table 6. Overall, the structural results and RMS fluctuations obtained using the semiempirical QM(PM3-AZI-ZN)/MM potential are in good agreement with results from the original PM3, and, more importantly, with the X-ray geometry, which further validates the performance of the computational model. Although the overall structural difference is small for the zinc metal complex in the gas phase and in the enzyme (Tables 3 and 6), some noticeable changes involve interactions between Zn^{2+} and azide ion. Specifically, the Zn−N1 distance (r_{14}) is increased by 0.03 Å in the enzyme active site (1.83 Å) in comparison with that for the [Zn(MeIm)$_3$−(N$_3$)]$^+$ complex in the gas phase (1.80 Å). This leads to reduced contributions from resonance structure **1**, which is reflected by a shortening of the N1−N2 bond length (r_{12}) by 0.01 Å, and elongation of the N2−N3 distance (r_{23}) by 0.01 Å. The geometrical trends are more sensitively accompanied by charge migrations from the metal back to N3 atom of azide as shown in the last two

TABLE 7: Calculated and Experimental Antisymmetric Vibrational Frequencies and Shifts for the Azide Ion in Carbonic Anhydrase[a]

	ω_3				$\Delta\omega_3$ (reference → CA-II)		
	gas	water	complex	CA-II	gas	water	complex
NMA	2037	2052	2209	2168	131	117	−41
1DW	2048	2074	2215	2161	113	87	−54
ACF	(2048)[b]	2086		2142	94	56	
exptl	1987[c]	2049[d]		2094[e]	107	45	

[a] The vibrational frequencies in the gas phase, water, and the metal complex, $[Zn(MeIm)_3-N_3]^+$, are also listed for reference. All frequencies are given in wavenumbers (cm^{-1}). [b] 1DW is used since the autocorrelation function was not computed for azide in the gas phase. [c] Reference 9. [d] Reference 21. [e] Reference 7.

columns of Table 5; the net partial charge of the azide ion increases from −0.062 to −0.123 au. Consequently, the participation of N1 atom in the antisymmetric stretching vibration is slightly recovered and the resulting vibrational frequency is decreased. The results indicate that the dynamics of protein modulates the participation of the resonance structures of the azide ion and is reflected in the observed spectral shifts and relaxation time.

The present molecular dynamics simulations employing a combined QM/MM potential reproduce the experimentally measured blue shift of the antisymmetric stretching frequency of an azide ligand in going from aqueous solution to the protein active site (Table 7). Normal mode analyses tend to overestimate the absolute antisymmetric vibrational frequency as well as the frequency shifts in comparison with experiment. The best results are obtained by including anharmonicity and coupling with the environment in 1DW and ACF calculations (Figure 2). The computed antisymmetric frequency for the azide ion in CA-II is 2161 cm^{-1} using the 1DW method by averaging over 250 protein configurations saved along the molecular dynamics trajectory, and it is 2142 cm^{-1} from the power spectrum of the autocorrelation function of the fluctuating coordinate (Table 7), which may be compared with the experimental value of 2094 cm^{-1}.[7] Importantly, the frequency shifts for the azide ion in going from aqueous solution into the CA-II active site are 87 and 56 cm^{-1} from the 1DW and ACF calculations, which are in excellent accord with the experimental result of 45 cm^{-1}.[7] The computed frequency shift (94−113 cm^{-1}) from the gas phase to the enzyme is also in good accord with experiment (107 cm^{-1}).

It is interesting to note that although a blue shift in the azide antisymmetric vibration from water to CA-II is observed, both computationally and experimentally, the origin of the shift is predominantly due to the change of the electronic structure of the azide ion through coordination to the metal ion, resulting in localization of the $N^{2-}-N^+\equiv N$ resonance structure (see above). The protein environment in fact attenuates the spectral shift by partially restoring the valence bond character of the electronic structure of an isolated azide and induces about −50 cm^{-1} of red shift relative to that of the $Zn(ImMe)_3^{2+}-N_3^-$ complex. This trend is also consistent with the changes in geometry and partial charges noted above. Thus, our computational results demonstrate that the increased contribution from the triple-bonded valence bond structure in the active site is responsible for the observed blue shift in azide antisymmetric vibration from water to CA-II, which has been suggested in the work of Lim et al.[7]

The results from QM/MM molecular dynamics simulations show that the instantaneous interactions between the azide ligand and the neighboring amino acid residues modify the potential

TABLE 8: Computed Interaction Distances and Experimental Values from the X-ray Structure for Key Residues in the Active Site[a]

interaction	PM3-AZI-ZN	PM3	X-ray[b]
Thr199 (OG1)-N1	3.3	3.5	3.2
Thr199 (N)-N1	4.0	4.3	4.2
Thr199 (N)-N2	3.5	3.5	3.7
Thr199 (N)-N3	3.3	2.9	3.4
Thr199(OG1)-Glu106(OE1)	2.8	2.7	2.5
Thr200(OG1)-N1	3.1	3.3	4.4
Thr200(N)-N1	3.6	4.0	4.7
Thr200(N)-N2	4.1	3.9	4.8
Thr200(N)-N3	4.7	4.1	5.1

[a] Atom numbers are shown in Figure 4. Distances are given in angstroms and the standard errors of the averaged distances are about 0.2 Å. [b] Reference 12.

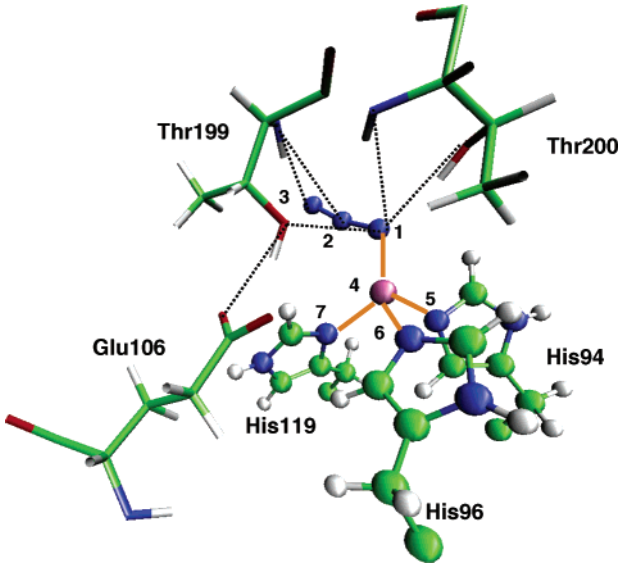

Figure 4. Schematic view of key interactions in the active site of carbonic anhydrase II.

energy surface of the azide ion in CA-II. These interactions are shown in the average distances between the azide ligand and active site residues. Table 8 lists calculated distances between atoms participating in key hydrogen-bonding interactions in the active site, along with the distances determined in the X-ray structure. We have highlighted the interactions with average distances less than 3.6 Å in Figure 4. Hydrogen-bonding interactions of the coordinating N1 atom of azide with the backbone amide hydrogen and the hydroxyl hydrogen of Thr200 can induce electronic polarization at the N1 position and stabilize the localized resonance structure **1**. However, the close proximity of the OG1 atom of Thr199 near N1 has the opposite effect. We attribute the migration of electron density from the N1 to the N3 atom in CA-II active site in comparison with the charge distribution of the $[Zn(MeIm)_3-(N_3)]^+$ complex in the gas phase to be the repulsive interaction between the ligand N1 atom and the OG1 atom of Thr199 and the strongly attractive hydrogen-bonding interactions between N3 and the backbone amine hydrogen of Thr199. These structural features from molecular dynamics simulations confirm the proposal that Thr199 plays a major role in modulating the charge distribution of the ligand, which in turn affects the admixture of valence bond structures and the ω_3 frequency in the active site of CA-II.[7]

5.3. Vibrational Energy Relaxation Time. The vibrational energy relaxation time for the azide antisymmetric stretch mode in water and in CA-II has been determined from the Fourier transform of the fluctuating force autocorrelation function (ACF)

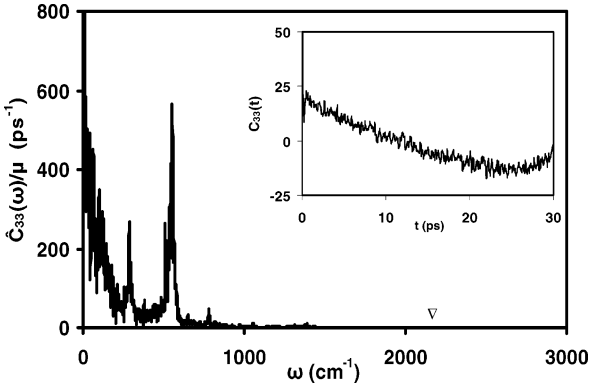

Figure 5. Power spectrum of the autocorrelation function (shown in the inset) of the fluctuating force on the antisymmetric stretch vibrational coordinate of azide in carbonic anhydrase II. The autocorrelation function in the inset was obtained by averaging over three independent trajectories, in which the azide geometry is fixed at its equilibrium value in the enzyme. The oscillator frequency at 2142 cm^{-1} is indicated by the "∇" mark.

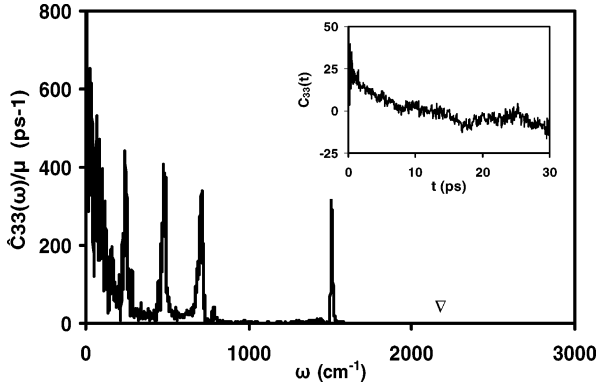

Figure 6. Power spectrum of the autocorrelation function (shown in the inset) of the fluctuating force on the antisymmetric stretch vibrational coordinate of azide in carbonic anhydrase II when only the antisymmetric stretch coordinate is constrained at its equilibrium value of $q_3 = -0.1159$ Å. The autocorrelation function in the inset was obtained by averaging over three independent trajectories.

of the force along the antisymmetric stretching coordinate, q_3. Here, the molecular dynamics simulations are performed with fixed azide equilibrium geometry in the corresponding environment.[86] In each case, the classical time-correlation function of the fluctuating force, $\langle \delta F_q(t) \delta F_q(0) \rangle_{cl}$, was obtained by averaging over three trajectories, each of which consists of 50 ps molecular dynamics simulations (1 fs time step since the azide geometry has been fixed). Following the procedure described by Bu and Straub,[86] the Fourier transform of the ACF has been smoothed by locally averaging over five data points, which yields an average power spectrum and a value at the frequency of the antisymmetric vibration of azide. Figure 5 shows the power spectrum and the ACF of the fluctuating force along the antisymmetric coordinate of azide in the enzyme (the results for azide in water are not shown).

Using the values of the power spectra at the oscillator frequencies in the protein (2142 cm^{-1}) and in water (2086 cm^{-1}), we obtain T_1 values of 14.5 and 4.7 ps, respectively, using the Landau−Teller formula, eq 16,[75,78] which correspond to the use of the harmonic correction factor in eq 14, following a mechanism of vibrational relaxation through Fermi resonance with a bath vibration.[79,84] This, however, is unlikely since there is no bath vibration, either in aqueous solution or in the protein, having frequencies in the range of 2100 cm^{-1}. Thus, it is important to make the necessary quantum corrections corresponding to a reasonable mechanism for the azide antisymmetric vibrational relaxation.

It is useful to examine the fluctuating force−force ACF obtained with the constraint of the antisymmetric coordinate only. Thus, other vibrational modes, including the azide symmetric stretch (q_1) and angle bending mode (q_2), can also be determined. Figure 6 shows the power spectrum for the fluctuating force−force ACF along the azide antisymmetric coordinate from simulations with only the antisymmetric coordinate constrained at $q_3 = -0.1159$ Å (see Figure 3). In the high-frequency region above 500 cm^{-1}, the most noticeable peaks are at 1510 and 790 cm^{-1} corresponding, respectively, to the symmetric stretch and angle bending of the azide ion. The peaks located at 250 and 495 cm^{-1} can be assigned, respectively, to the Zn−N−N angle bending and the Zn−azide stretch in comparison with normal mode analysis. The presence of these vibrational modes associated with the oscillator suggests that they are strongly coupled to the antisymmetric stretch vibration. Interestingly, similar features have also been observed in the study of the vibrational energy relaxation of a C−D stretch in the terminal methyl group of Met80 in cytochrome *c* protein,[86] in which the vibrational modes strongly coupled to the C−D stretch are all in the neighborhood of the Met80 residue, including the methylene bending and the stretch and angle bending associated with the S−C bond of Met80.

TABLE 9: Estimated Quantum Correction Factors (QCF) and the Corresponding Relaxation Times T_1 (ps) for the Antisymmetric Vibration Mode of Azide Ion in Water and in Carbonic Anhydrase

	QCF		T_1 (ps)	
method	water	CA-II	water	CA-II
$Q_H(\omega_0)$	10.07	10.34	4.67	14.51
$Q_H(\omega_1)Q_H(\omega_0 - \omega_1)/Q_H(\omega_0)$	1.71	2.26	2.56	6.42
$Q_H(\omega_1)Q_{HS}(\omega_0 - \omega_1)/Q_H(\omega_0)$	1.97	2.71	2.38	5.36
$Q_H(2\omega_2)Q_H(\omega_0 - 2\omega_2)/Q_H(\omega_0)$	2.25	2.14	2.07	6.78
$Q_H(2\omega_2)Q_{HS}(\omega_0 - 2\omega_2)/Q_H(\omega_0)$	2.72	2.47	1.72	5.87
exptl			1.2 ± 0.4[a] 0.81 ± 0.02[b]	2.8 ± 0.4[a]

[a] References 21 and 7. [b] Reference 19.

Recently, the mechanism of vibrational energy relaxation of azide ion in water has been investigated by Morita and Kato by including intramolecular vibrational redistribution (IVR) along with charge polarization effects.[29] It was found that the direct relaxation of the antisymmetric vibration to the ground state and the IVR to the Fermi resonance states (the mixture of the symmetric stretch, |100>, and the overtone of the N−N−N bend, |020>) have nearly equal contributions to the overall relaxation rate.[29] Analogously, in the study of vibrational relaxation of HOD in D_2O, Rey and Hynes showed that the O−H relaxation occurs via an intramolecular relaxation pathway of $|001\rangle \rightarrow |020\rangle$ to the overtone of the HOD bend.[80] IVR provides an important mechanism for vibrational relaxation. Thus, following the analyses and relaxation mechanism of Morita and Kato,[29] we can use the semiclassical quantum correction method proposed by Skinner and Park[84] to estimate the overall quantum correction factor for the azide relaxation in carbonic anhydrase II and in water.

Table 9 lists the estimated QCFs and the corresponding relaxation time both in water and in the enzyme CA-II. The uncorrected classical results, which correspond to using harmonic correction factors of $Q = Q_H(\omega_0) = 10.34$ and 10.07 at the azide antisymmetric vibrational frequencies (quantum oscillator) in CA-II and in water (quantum harmonic bath). For the mechanism of intramolecular vibration redistribution, if one

quantum from the azide antisymmetric stretch at frequency ω_0 in the enzyme (or in water) is transferred to one quantum of the symmetric stretch of azide at $\omega_i = 1510$ cm^{-1} ($\omega_i = 1687$ cm^{-1} in water) with the remaining $\omega_0 - \omega_i \approx 630$ (400) cm^{-1} being accepted by one quantum of a low-frequency harmonic vibration in the enzyme ($Q_H(\omega_0 - \omega_i)$) or by translation and rotational modes of the bath ($Q_{HS}(\omega_0 - \omega_i)$), the total quantum correction factor would be $Q = Q_H(\omega_i)Q_H(\omega_0 - \omega_i)$ or $Q = Q_H(\omega_i)Q_{HS}(\omega_0 - \omega_i)$, respectively.[84] We also list the quantum correction factors for the energy transfer to the overtone of the azide angle bending in Table 9 for comparison. Thus, depending on the specific mechanism and quantum correction factor used, the estimated azide vibration relaxation time is about 1.7 to 2.6 ps in water and about 5.4 to 6.8 ps in CA-II. This may be compared with the experimental results of 1.2 ps[10,18,21,22] in water and 2.8 ps in CA-II.[7] We note that another experimental study yielded a T_1 value of 0.81 ps for azide ion in water,[19] somewhat faster than the previous result. Thus, the present QM/MM molecular dynamics simulations overestimate the absolute values of the relaxation time by a factor of about 2 for azide ion in water and in the CA-II enzyme. Significantly, the present QM/MM molecular dynamics simulations correctly reproduced the experimental finding that the azide antisymmetric vibrational relaxation time is about 2.5 times greater in the enzyme than that in water.

6. Conclusions

Combined QM/MM molecular dynamics simulations have been carried out to investigate the vibrational frequency shift for the azide antisymmetric stretch mode induced by aqueous solvation and by the enzyme carbonic anhydrase. Furthermore, the vibrational energy relaxation time has been determined both in water and in the enzyme. In this work the oscillator and the enzyme active site is treated explicitly by quantum mechanics. Thus, the dynamical change of the potential energy surface of the oscillator can be adequately represented. Although the average geometry of the azide ion is symmetric in aqueous solution, the instantaneous solute−solvent interactions induce localization of the charge density and greater contributions from the resonance structures having triple bond characters. Consequently, the vibrational frequency is blue shifted, and the best estimate of the frequency shift that include anharmonicity is 38 cm^{-1} in accord with the experimental result of 62 cm^{-1}. The azide antisymmetric stretch vibration is further shifted by about 50 cm^{-1} from experimental studies, while our computation result is 56 cm^{-1}. The origin of the protein-induced blue shift for azide ion from water to carbonic anhydrase is due to a combination of ligand binding to the zinc metal ion in the active site and protein dynamical interactions. The former makes the dominant contribution by stabilizing the $N{\equiv}N^+-N^{2-}$ ionic state through ligand−metal coordination, which involves significant charge transfer from the azide ligand to the Zn^{2+} ion. The increased admixture of the $N{=}N^+{=}N^{2-}$ valence bond structure strengthens the triple bond stretch character in the metal complex, resulting in a predicted blue shift of about 130 to 160 cm^{-1} relative to an isolated azide ion in the gas phase. The interactions of the metal-bound azide ion with amino acid residues in the active site of carbonic anhydrase II attenuate the ligand−metal bonding, recovering some of the $N^-{=}N^+{=}N^-$ valence bond character, and reduce the antisymmetric vibration spectral shift by about −50 cm^{-1}.

The vibrational energy relaxation time was studied by computing the fluctuating force autocorrelation functions along the antisymmetric stretch coordinate both for azide ion in water and in the active site of carbonic anhydrase. Intramolecular vibrational redistribution provides a major doorway for energy relaxation in the enzyme, consistent with the mechanism obtained previously in a study of intramolecular vibration redistribution of azide ion in water by Morita and Kato.[29] Following this mechanism coupled with the quantum correction factor suggested by Skinner and Park,[84] we obtain vibrational relaxation times of about 2 ps in water and 6 ps in carbonic anhydrase, which may be compared with the experimental data of 1.2 and 2.8 ps,[7] respectively. Importantly, the change in relaxation time by a factor of 2.5 from water to the enzyme is correctly reproduced. The present study suggests that the modes that serve as a main pathway for accepting the vibrational energy of the antisymmetric mode are in close proximity to the oscillator, a finding that has also been observed in the C−D stretch vibrational relaxation in cytochrome *c* by Bu and Straub.[86]

Acknowledgment. We thank the National Institutes of Health for generous support of our research on enzyme kinetics. We thank Drs. Ricard Gelabert, John E. Straub, and Donald G. Truhlar for helpful discussions.

References and Notes

(1) Brooks, C. L., III.; Karplus, M.; Pettitt, B. M. *Adv. Chem. Phys.* **1988**, *71*, 1−259.
(2) Frauenfelder, H.; McMahon, B. H.; Austin, R. H.; Chu, K.; Groves, J. T. *Proc. Nat. Acad. Sci. U.S.A.* **2001**, *98*, 2370−2374.
(3) Hochstrasser, R. M. *J. Chem. Educ.* **1998**, *75*, 559−564.
(4) Jimenez, R.; Fleming, G. R.; Kumar, P. V.; Maroncelli, M. *Nature (London)* **1994**, *369*, 471−473.
(5) Lim, M.; Jackson, T. A.; Anfinrud, P. A. *Science* **1995**, *269*, 962−966.
(6) Pal, S. K.; Peon, J.; Zewail, A. H. *Proc. Nat. Acad. Sci. U.S.A.* **2002**, *99*, 15297−15302.
(7) Lim, M.; Hamm, P.; Hochstrasser, R. M. *Proc. Natl. Acad. Sci. U.S.A.* **1998**, *95*, 15315−15320.
(8) Asplund, M. C.; Lim, M.; Hochstrasser, R. M. *Chem. Phys. Lett.* **2000**, *323*, 269−277.
(9) Polak, M.; Gruebele, M.; Saykally, R. J. *J. Am. Chem. Soc.* **1987**, *109*, 2884−2887.
(10) Hamm, P.; Lim, M.; Hochstrasser, R. M. *Phys. Rev. Lett.* **1998**, *81*, 5326−5329.
(11) Dobramysl, W.; Fritzer, H. P.; Harland, L.; Kettle, S. F. A. *Spectrochim. Acta, Part A* **1977**, *33A*, 221−226.
(12) Joensson, B. M.; Hakansson, K.; Liljas, A. *FEBS Lett.* **1993**, *322*, 186−190.
(13) Nair, S. K.; Christianson, D. W. *Eur. J. Biochem.* **1993**, *213*, 507−515.
(14) Teraoka, J.; Yamamoto, N.; Matsumoto, Y.; Kyogoku, Y.; Sugeta, H. *J. Am. Chem. Soc.* **1996**, *118*, 8875−8878.
(15) Varo, G.; Brown, L. S.; Needleman, R.; Lanyi, J. K. *Biochemistry* **1996**, *35*, 6604−6611.
(16) Tsubaki, M.; Mogi, T.; Hori, H. *J. Biochem. (Tokyo)* **1999**, *126*, 510−519.
(17) Waterland, M. R.; Kelley, A. M. *J. Phys. Chem. A* **2001**, *105*, 8385−8392.
(18) Owrutsky, J. C.; Kim, Y. R.; Li, M.; Sarisky, M. J.; Hochstrasser, R. M. *Chem. Phys. Lett.* **1991**, *184*, 368−374.
(19) Zhong, Q.; Steinhurst, D. A.; Carpenter, E. E.; Owrutsky, J. C. *Langmuir* **2002**, *18*, 7401−7408.
(20) Zhong, Q.; Baronavski, A. P.; Owrutsky, J. C. *J. Chem. Phys.* **2003**, *118*, 7074−7080.
(21) Li, M.; Owrutsky, J.; Sarisky, M.; Culver, J. P.; Yodh, A.; Hochstrasser, R. M. *J. Chem. Phys.* **1993**, *98*, 5499−5507.
(22) Heilweil, E. J.; Doany, F. E.; Moore, R.; Hochstrasser, R. M. *J. Chem. Phys.* **1982**, *76*, 5632−5634.
(23) Zhong, Q.; Owrutsky, J. C. *Chem. Phys. Lett.* **2004**, *383*, 176−180.
(24) Botschwina, P. *J. Chem. Phys.* **1986**, *85*, 4591−4593.
(25) Kaldor, U. *Int. J. Quantum Chem., Quantum Chem. Symp.* **1990**, *24*, 291−294.
(26) Fadini, A.; Schroeder, H. F.; Mueller, J. *Z. Anorg. Allg. Chem.* **1982**, *488*, 121−125.
(27) Ferrario, M.; Klein, M. L.; McDonald, I. R. *Chem. Phys. Lett.* **1993**, *213*, 537−540.

(28) Yarne, D. A.; Tuckerman, M. E.; Klein, M. L. *Chem. Phys.* **2000**, *258*, 163−169.
(29) Morita, A.; Kato, S. *J. Chem. Phys.* **1998**, *109*, 5511−5523.
(30) Briganti, F.; Iaconi, V.; Mangani, S.; Orioli, P.; Scozzafava, A.; Vernaglione, G.; Supuran, C. T. *Inorg. Chim. Acta* **1998**, *275*−*276*, 295−300.
(31) Liang, J. Y.; Lipscomb, W. N. *Biochemistry* **1988**, *27*, 8676−8682.
(32) Aaqvist, J.; Warshel, A. *J. Mol. Biol.* **1992**, *224*, 7−14.
(33) Jackman, J. E.; Merz, K. M., Jr.; Fierke, C. A. *Biochemistry* **1996**, *35*, 16421−16428.
(34) Lu, D.; Voth, G. A. *J. Am. Chem. Soc.* **1998**, *120*, 4006−4014.
(35) Lu, D.; Voth, G. A. *Proteins: Struct., Funct., Genet.* **1998**, *33*, 119−134.
(36) Toba, S.; Colombo, G.; Merz, K. M., Jr. *J. Am. Chem. Soc.* **1999**, *121*, 2290−2302.
(37) Isaev, A. N. *THEOCHEM* **2002**, *582*, 195−203.
(38) Chen, H.; Li, S.; Jiang, Y. *J. Phys. Chem. A* **2003**, *107*, 4652−4660.
(39) Cui, Q.; Karplus, M. *J. Phys. Chem. B* **2003**, *107*, 1071−1078.
(40) Smedarchina, Z.; Siebrand, W.; Fernandez-Ramos, A.; Cui, Q. *J. Am. Chem. Soc.* **2003**, *125*, 243−251.
(41) Merz, K. M., Jr.; Banci, L. *J. Phys. Chem.* **1996**, *100*, 17414−17420.
(42) Krauss, M.; Garmer, D. R. *J. Am. Chem. Soc.* **1991**, *113*, 6426−6435.
(43) Sola, M.; Lledos, A.; Duran, M.; Bertran, J. *NATO ASI Ser., Ser. C* **1992**, *368*, 263−298.
(44) Aaqvist, J.; Fothergill, M.; Warshel, A. *J. Am. Chem. Soc.* **1993**, *115*, 631−635.
(45) Madura, J. D.; Nakajima, Y.; Hamilton, R. M.; Wierzbicki, A.; Warshel, A. *Struct. Chem.* **1996**, *7*, 131−138.
(46) Garmer, D. R. *J. Phys. Chem. B* **1997**, *101*, 2945−2953.
(47) Merz, K. M., Jr.; Hoffmann, R.; Dewar, M. J. S. *J. Am. Chem. Soc.* **1989**, *111*, 5636−5649.
(48) Merz, K. M., Jr. *J. Mol. Biol.* **1990**, *214*, 799−802.
(49) Zheng, Y. J.; Merz, K. M., Jr. *J. Am. Chem. Soc.* **1992**, *114*, 10498−10507.
(50) Rossi, K. A.; Merz, K. M., Jr.; Smith, G. M.; Baldwin, J. J. *J. Med. Chem.* **1995**, *38*, 2061−2069.
(51) Hartsough, D. S.; Merz, K. M., Jr. *J. Phys. Chem.* **1995**, *99*, 11266−11275.
(52) Field, M. J.; Bash, P. A.; Karplus, M. *J. Comput. Chem.* **1990**, *11*, 700−733.
(53) Warshel, A. *Computer Modeling of Chemical Reactions in Enzymes and Solutions*; Wiley: New York, 1991.
(54) Singh, U. C.; Kollman, P. A. *J. Comput. Chem.* **1986**, *7*, 718−730.
(55) Gao, J.; Xia, X. *Science* **1992**, *258*, 631−635.
(56) Gao, J. In *Reviews in Computational Chemistry*; Lipkowitz, K. B., Boyd, D. B., Eds.; VCH: New York, 1995; Vol. 7, pp 119−185.
(57) Gao, J.; Truhlar, D. G. *Annu. Rev. Phys. Chem.* **2002**, *53*, 467−505.
(58) Gao, J.; Luque, F. J.; Orozco, M. *J. Chem. Phys.* **1993**, *98*, 2975−2982.
(59) Garcia-Viloca, M.; Truhlar, D. G.; Gao, J. *J. Mol. Biol.* **2003**, *327*, 549−560.
(60) Amara, P.; Field, M. J. In *Computational Molecular Biology*; Leszczynski, J., Ed.; Elsevier: Amsterdam, 1999; pp 1−33.
(61) MacKerell, A. D., Jr.; Bashford, D.; Bellott, M.; Dunbrack, R. L.; Evanseck, J. D.; Field, M. J.; Fischer, S.; Gao, J.; Guo, H.; Ha, S.; Joseph-McCarthy, D.; Kuchnir, L.; Kuczera, K.; Lau, F. T. K.; Mattos, C.; Michnick, S.; Ngo, T.; Nguyen, D. T.; Prodhom, B.; Reiher, W. E., III; Roux, B.; Schlenkrich, M.; Smith, J. C.; Stote, R.; Straub, J.; Watanabe, M.; Wiorkiewicz-Kuczera, J.; Yin, D.; Karplus, M. *J. Phys. Chem. B* **1998**, *102*, 3586−3616.
(62) Gao, J. *ACS Symp. Ser.* **1994**, *569*, 8−21.
(63) Freindorf, M.; Gao, J. *J. Comput. Chem.* **1996**, *17*, 386−395.
(64) Gao, J.; Amara, P.; Alhambra, C.; Field, M. J. *J. Phys. Chem. A* **1998**, *102*, 4714−4721.
(65) Garcia-Viloca, M.; Gao, J. *Theor. Chem. Acc.* **2004**, *111*, 280−286.
(66) Frisch, M. J.; Trucks, G. W.; Schlegel, H. B.; Scuseria, G. E.; Robb, M. A.; Cheeseman, J. R.; Zakrzewski, V. G.; Montgomery, J. A., Jr.; Stratmann, R. E.; Burant, J. C.; Dapprich, S.; Millam, J. M.; Daniels, A. D.; Kudin, K. N.; Strain, M. C.; Farkas, O.; Tomasi, J.; Barone, V.; Cossi, M.; Cammi, R.; Mennucci, B.; Pomelli, C.; Adamo, C.; Clifford, S.; Ochterski, J.; Petersson, G. A.; Ayala, P. Y.; Cui, Q.; Morokuma, K.; Malick, D. K.; Rabuck, A. D.; Raghavachari, K.; Foresman, J. B.; Cioslowski, J.; Ortiz, J. V.; Stefanov, B. B.; Liu, G.; Liashenko, A.; Piskorz, P.; Komaromi, I.; Gomperts, R.; Martin, R. L.; Fox, D. J.; Keith, T.; Al-Laham, M. A.; Peng, C. Y.; Nanayakkara, A.; Gonzalez, C.; Challacombe, M.; Gill, P. M. W.; Johnson, B. G.; Chen, W.; Wong, M. W.; Andres, J. L.; Head-Gordon, M.; Replogle, E. S.; Pople, J. A. *Gaussian 98*; Gaussian, Inc.: Pittsburgh, PA, 1998.
(67) Stewart, J. J. P. *J. Comput.-Aided Des.* **1990**, *4*, 1−105.
(68) Garcia-Viloca, M.; Corchado, J. C.; Alhambra, C.; Villa, J.; Gao, J.; Truhlar, D. G. 0.1 ed.; University of Minnesota: Minneapolis, Mn, 2002.
(69) Brooks, B. R.; Bruccoleri, R. E.; Olafson, B. D.; States, D. J.; Swaminathan, S.; Karplus, M. *J. Comput. Chem.* **1983**, *4*, 187.
(70) Alhambra, C.; Corchado, J.; Sanchez, M. L.; Garcia-Viloca, M.; Gao, J.; Truhlar, D. G. *J. Phys. Chem. B* **2001**, *105*, 11326−11340.
(71) Press, W. H.; Flannery, B. P.; Teukolsky, S. A.; Vetterling, W. T. *Numerical Recipes*; University of Cambridge: New York, 1992.
(72) Hamilton, I. P.; Light, J. C. *J. Chem. Phys.* **1986**, *84*, 306−317.
(73) Wang, J.; Boyd, R. J.; Laaksonen, A. *J. Chem. Phys.* **1996**, *104*, 7261−7269.
(74) Alhambra, C.; Byun, K.; Gao, J. *ACS Symp. Ser.* **1998**, *712*, 35−49.
(75) Zwanzig, R. *J. Chem. Phys.* **1961**, *34*, 1931−1935.
(76) Whitnell, R. M.; Wilson, K. R.; Hynes, J. T. *J. Phys. Chem.* **1990**, *94*, 8625−8628.
(77) Whitnell, R. M.; Wilson, K. R.; Hynes, J. T. *J. Chem. Phys.* **1992**, *96*, 5354−5369.
(78) Oxtoby, D. W. *Adv. Chem. Phys.* **1981**, *47*, 487−519.
(79) Bader, J. S.; Berne, B. J. *J. Chem. Phys.* **1994**, *100*, 8359−8366.
(80) Rey, R.; Hynes, J. T. *J. Chem. Phys.* **1996**, *104*, 2356−2368.
(81) Sun, Y. C.; Gai, H.; Voth, G. A. *J. Chem. Phys.* **1994**, *100*, 3247−3251.
(82) Jang, S.; Pak, Y.; Voth, G. A. *J. Phys. Chem. A* **1999**, *103*, 10289−10293.
(83) Egorov, S. A.; Skinner, J. L. *J. Chem. Phys.* **1996**, *105*, 7047−7058.
(84) Skinner, J. L.; Park, K. *J. Phys. Chem. B* **2001**, *105*, 6716−6721.
(85) Sagnella, D. E.; Straub, J. E.; Jackson, T. A.; Lim, M.; Anfinrud, P. A. *Proc. Natl. Acad. Sci. U.S.A.* **1999**, *96*, 14324−14329.
(86) Bu, L.; Straub, J. E. *Biophys. J.* **2003**, *85*, 1429−1439.
(87) Bu, L.; Straub, J. E. *J. Phys. Chem. B* **2003**, *107*, 12339−12345.
(88) Sagnella, D. E.; Straub, J. E. *Biophys. J.* **1999**, *77*, 1.
(89) Egorov, S. A.; Everitt, K. F.; Skinner, J. L. *J. Phys. Chem. A* **1999**, *103*, 9494−9499.
(90) Gao, J.; Freindorf, M. *J. Phys. Chem. A* **1997**, *101*, 3182−3188.
(91) Eichinger, M.; Tavan, P.; Hutter, J.; Parrinello, M. *J. Chem. Phys.* **1999**, *110*, 10452−10467.
(92) Rothlisberger, U.; Carloni, P.; Doclo, K.; Parrinello, M. *J. Biol. Inorg. Chem.* **2000**, *5*, 236−250.
(93) Stewart, J. J. P. *J. Comput. Chem.* **1989**, *10*, 209−220.
(94) Jorgensen, W. L.; Chandrasekhar, J.; Madura, J. D.; Impey, R. W.; Klein, M. L. *J. Chem. Phys.* **1983**, *79*, 926−935.
(95) Dewar, M. J. S.; Zoebisch, E. G.; Healy, E. F.; Stewart, J. J. P. *J. Am. Chem. Soc.* **1985**, *107*, 3902−3909.
(96) Brauer, M.; Kunert, M.; Dinjus, E.; Klussmann, M.; Doring, M.; Gorls, H.; Anders, E. *THEOCHEM* **2000**, *505*, 289−301.
(97) Corchado, J. C.; Espinosa-Garcia, J.; Hu, W.-P.; Rossi, I.; Truhlar, D. G. *J. Phys. Chem.* **1995**, *99*, 687−694.
(98) Elstner, M.; Cui, Q.; Munih, P.; Kaxiras, E.; Frauenheim, T.; Karplus, M. *J. Comput. Chem.* **2003**, *24*, 565−581.
(99) Hockney, R. W. *Methods Comput. Phys.* **1970**, *9*, 136−211.
(100) Nose, S. *J. Chem. Phys.* **1984**, *81*, 511.
(101) Hoover, W. G. *Phys. Rev. A* **1985**, *31*, 1695.
(102) Andersen, H. C. *J. Chem. Phys.* **1980**, *72*, 2384.
(103) Ryckaert, J. P.; Cicotti, G.; Berendsen, H. J. C. *J. Comput. Phys.* **1977**, *23*, 327−337.
(104) Verlet, L. *Phys. Rev.* **1967**, *159*, 98.
(105) Steiner, H.; Jonsson, B. H.; Lindskog, S. *Eur. J. Biochem. 59*, 253−259.
(106) Silverman, D. N.; Lindskog, S. *Acc. Chem. Res.* **1988**, *21*, 30−36.
(107) Brooks, C. L., III; Karplus, M. *J. Chem. Phys.* **1983**, *79*, 6312−6325.
(108) Brooks, C. L., III; Karplus, M. *J. Mol. Biol.* **1989**, *208*, 159−181.
(109) Le Borgne, C.; Illien, B.; Beignon, M.; Chabanel, M. *Phys. Chem. Chem. Phys.* **1999**, *1*, 4701−4706.